isolated patterns—are related to the fact that molten silicon has a viscosity of 0.003 $cm^2 s^{-1}$, which is one-third that of water (0.01 $cm^2 s^{-1}$; ref. 10). This low viscosity enables the molten silicon to flow rapidly into all crevasses, filling them completely and conforming to the mould. Furthermore, silicon, like water, has a liquid phase density (2.52 $g cm^{-3}$) greater than its solid phase (2.32 $g cm^{-3}$; ref. 11). The transformation from liquid to solid causes the silicon volume to expand about 3% in each direction. However, during LADI the mould was at a lower temperature than that of molten silicon, so the shrinking of silicon caused by the temperature drop can offset the expansion of silicon from liquid phase to the solid.

LADI can be applied to other materials. We have deposited, by chemical vapour deposition (CVD), a 230 nm polysilicon layer on top of a 200 nm thick silicon dioxide layer grown on a silicon substrate. Nanostructures have been patterned in the polysilicon layer by LADI (for example, Fig. 4b). The results are the same as that of crystalline silicon, except that the polysilicon has a slightly lower melting energy than crystalline silicon[7]. This indicates that LADI may become a good tool to directly pattern nanoscale gates for metal-oxide-semiconductor field-effect transistors (MOSFETs).

The velocity, acceleration, force, pressure, and Reynolds number involved in LADI of silicon can be estimated to provide further information about the process. In our experiments the imprint depth was 110 nm and the imprint time was around 250 ns. For simplicity, we assume that the mould travelled a distance of 100 nm in 200 ns; however, this distance may be slightly overestimated owing to elastic distortion of the mould under pressure and the upward flow of liquid silicon. This leads to an average imprint velocity of about 0.5 $m s^{-1}$ and an average acceleration of 5×10^6 $m s^{-2}$—nearly a million times the gravitational acceleration. Because the mould has a weight of about 5.6 mg, the total force needed for the acceleration is about 28 N. For the given mould area (2.25 mm^2), the total pressure on the mould needed for the imprint is 1.7×10^6 Pa or about 17 atm. If we assume the liquid Si flow during LADI is one-dimensional and into a 140 nm opening at a speed of 0.5 $m s^{-1}$, then the Reynolds number is 0.23, which is quite small, indicating a laminar flow.

Finally, LADI can be extended to large areas, other materials, and other processes. The LADI area could be as large as a whole wafer (4 inch or 8 inch diameter), or a one-inch-square die (that die can be used to cover an entire wafer by step and repeat), provided that a uniform laser beam over a large area is available. Conventional nanoimprint has demonstrated excellent uniformity over a 4-inch wafer in a single step[2,3]. LADI also could be used for other materials beyond crystalline silicon and polysilicon, such as Ge, III–V compound semiconductors and dielectrics (a different laser wavelength would be needed). LADI could help to crystallize polysilicon further. LADI might be well suited for three-dimensional patterning (for example, forming a lens on a Si or glass surface), which is challenging to achieve by conventional lithography and etching. LADI could offer a unique method to fill tiny holes in a dielectric (for example, silicon dioxide) with silicon, and a unique means of flattening the surface of a semiconductor deposited on a dielectric. Both are difficult issues in integrated circuit fabrication. Many applications of LADI are yet to be explored. □

Received 7 January; accepted 1 May 2002; doi:10.1038/nature00792.

1. Ito, T. & Okazaki, S. Pushing the limits of lithography. *Nature* **406,** 1027–1031 (2000).
2. Rogers, J. A. & Mirkin, C. Emerging methods for micro- and nanofabrication. *Mater. Res. Bull.* **26,** (2001).
3. Chou, S. Y., Krauss, P. R. & Renstrom, P. J. Imprint lithography with 25-nanometer resolution. *Science* **272,** 85–87 (1996).
4. Chou, S. Y. & Zhuang, L. Lithographically induced self-assembly of periodic polymer micropillar arrays. *J. Vac. Sci. Technol. B* **17,** 3197–3202 (1999).
5. Silvesrelli, P. L., Alavi, A., Parrinello, M. & Frenkel, D. Ab initio molecular dynamics simulation of laser melting of silicon. *Phys. Rev. Lett.* **77,** 3149–3152 (1996).
6. Ivlev, G. D. & Gatskevich, E. I. Liquid phase reflectivity under conditions of laser induced melting. *Semiconductors* **34,** 759–762 (2000).
7. Poute, J. M. & Mayer, J. *Laser Annealing of Semiconductors* (Academic, New York, 1982).
8. Carey, P. G. & Sigmon, T. W. In-situ doping of silicon using gas immersion laser doping (GILD). *Appl. Surf. Sci.* **43,** 325–332 (1989).
9. Weiner, K. H. & Sigmon, T. W. Thin-base bipolar transistor fabrication using gas immersion laser doping. *IEEE Electr. Device Lett.* **10,** 260–263 (1989).
10. Glazov, V. M., Chizhevskaya, S. N. & Glagoleva, N. N. *Liquid Semiconductors* (Plenum, New York, 1969).
11. Langen, M., Hibiya, T., Eguchi, M. & Egry, I. Measurement of the density and the thermal expansion coefficient of molten silicon using electromagnetic levitation. *J. Cryst. Growth* **186,** 550–556 (1998).

Acknowledgements

We thank Y. Zhan for his contributions in the initial phase of the work, Z. Suo for help with the discussion of the Reynolds number, and the US Defense Advanced Research Program Agency (DARPA), the Office of Naval Research (ONR) and the Army Research Office (ARO, through an equipment grant) for their partial financial support of the project.

Competing interests statement

The authors declare that they have no competing financial interests.

Correspondence and requests for materials should be addressed to S.Y.C. (e-mail: chou@ee.princeton.edu).

Growth of early continental crust controlled by melting of amphibolite in subduction zones

Stephen Foley*, Massimo Tiepolo† & Riccardo Vannucci†

** Institut für Geologische Wissenschaften, Universität Greifswald, F.L. Jahnstrasse 17a, D-17487 Greifswald, Germany*
† Dipartimento di Scienze della Terra, Università di Pavia and CNR- Istituto di Geoscienze e Georisorse (IGG) - Sezione di Pavia, Via Ferrata 1, I-27100 Pavia, Italy

It is thought that the first continental crust formed by melting of either eclogite or amphibolite, either at subduction zones[1] or on the underside of thick oceanic crust[2]. However, the observed compositions of early crustal rocks and experimental studies have been unable to distinguish between these possibilities[3–5]. Here we show a clear contrast in trace-element ratios of melts derived from amphibolites and those from eclogites. Partial melting of low-magnesium amphibolite can explain the low niobium/tantalum and high zirconium/samarium ratios in melts, as required for the early continental crust, whereas the melting of eclogite cannot. This indicates that the earliest continental crust formed by melting of amphibolites in subduction-zone environments and not by the melting of eclogite or magnesium-rich amphibolites in the lower part of thick oceanic crust. Moreover, the low niobium/tantalum ratio seen in subduction-zone igneous rocks of all ages is evidence that the melting of rutile-eclogite has never been a volumetrically important process.

The early continental crust is characterized by the tonalite–trondhjemite–granodiorite gneisses (TTG) of Archaean terrains[3]. Their compositions have been explained as the products of magmatic processes, namely melting of basaltic source rocks in the form of either eclogite or amphibolite[1,4–5]. However, it is debated whether the melting process occurred principally in subduction zones[1] or on the underside of oceanic crust[2] that may have been much thicker in the Archaean owing to higher geothermal gradients.

TTG gneisses have low Nb/Ta and high Zr/Sm ratios relative to modern oceanic basalts and mantle rocks. They share these charac-

teristics with modern adakites (Fig. 1a), which are, on the basis of experimental petrology and major- and trace-element patterns, thought to originate by melting of the subducting basalt slab, and may thus be rare modern analogues of Archaean crust-building magmatism[6]. Subducting basalt would be much more likely to melt during Archaean times because of the higher geothermal gradient and probably lower average age of oceanic crust being subducted[7]. Any crust produced by this process would, therefore, have been much more voluminous than adakites are today. The alternative model of melting of lower levels of thickened oceanic crust has no direct modern analogue: thick oceanic plateaux do occur and serve as a model for the Archaean oceanic crust[8], but the lower thermal gradients today prevent them from melting. Nevertheless, there are differences between these two models for the origin of TTG gneisses: subducting crust could conceivably melt as amphibolite or eclogite, but its average composition would generally be that of fractionated basalt; more than 90% of mid-ocean-ridge basalts (MORBs) have Mg number (Mg# = 100 Mg/(Mg + Fe)) between 50 and 65. The underside of thick oceanic crust would have higher Mg# because it consists of a high proportion of cumulates[8]. Furthermore, the thick crust would be formed by high-degree melts with very low water contents[9], and so the lower crust would consist largely of granulite and eclogite, not amphibolite. Hydrothermal alteration at ridges is

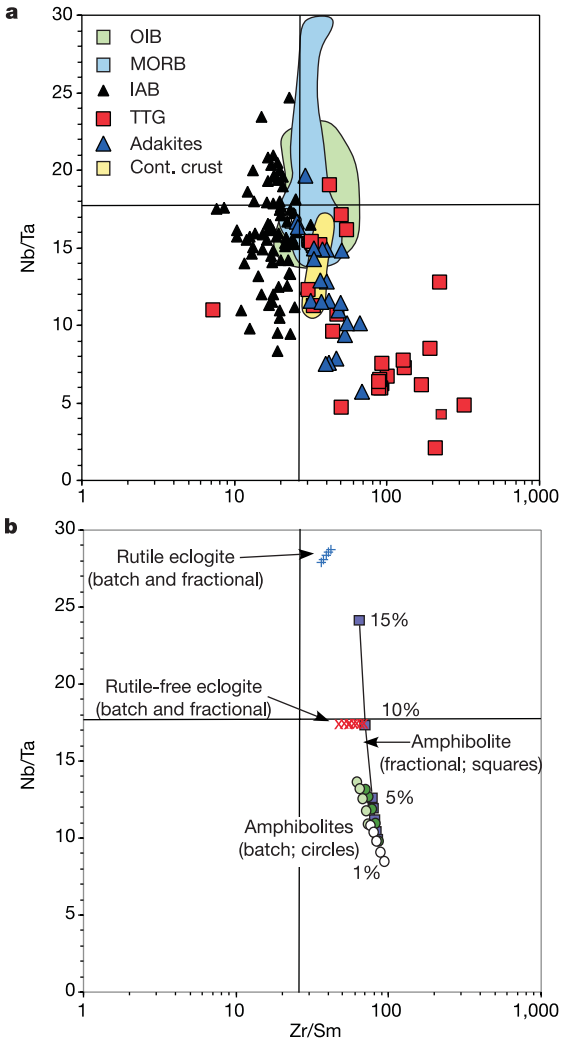

Figure 1 Nb/Ta ratios versus Zr/Sm ratios of natural rocks, compared to results of modelled melting of eclogites and amphibolites. **a**, The early continental crust represented by trondhjemite–tonalite–granodiorite gneisses (TTG) lie in the lower right quadrant with low Nb/Ta and high Zr/Sm, as do modern adakites. This trace-element signature differs from that of primitive mantle (at the intersection of the black lines), modern mid-ocean-ridge basalts (MORBs), ocean-island basalts (OIB) and island-arc basalts (IAB), all of which have lower Zr/Sm and/or higher Nb/Ta. The bulk continental crust also lies to the lower right, and may correspond to a TTG signature later diluted by crustal growth by other processes. **b**, Trace-element modelling of partial melting of eclogite and amphibolite using the new experimental partitioning data[11–15] shows that melts of eclogite bearing rutile (blue plus signs) lie in the upper right quadrant, and eclogites without rutile (red crosses) have unfractionated Nb/Ta. Rocks in the lower right quadrant may originate by 1–15% batch melting of amphibolite. Melting models were based on high-pressure experiments in which mineral modes were measured[4,5]; three different amphibolites were modelled, producing similar results: (1) 0.8 GPa (ref. 4) (white circles) with 40% amphibole (Am), 45% plagioclase (Plg) and 15% orthopyroxene; (2) 1.0 GPa (ref. 5) (light green circles) with 32% Am, 15% Plg, 28% garnet (Ga) and 25% clinopyroxene (Cpx); (3) 1.6 GPa (ref. 4) (dark green circles) with 17% Am, 15% Plg, 15% Ga and 52% Cpx. Purple squares are for pure fractional melting at 1.0 GPa, showing that only very low degree fractional melts could carry this trace-element signature. Partition coefficients used are for Plg with An_{45} and Am with Mg# = 45. The starting composition used for modelling was an average Archaean basalt from Sula Mountain[30].

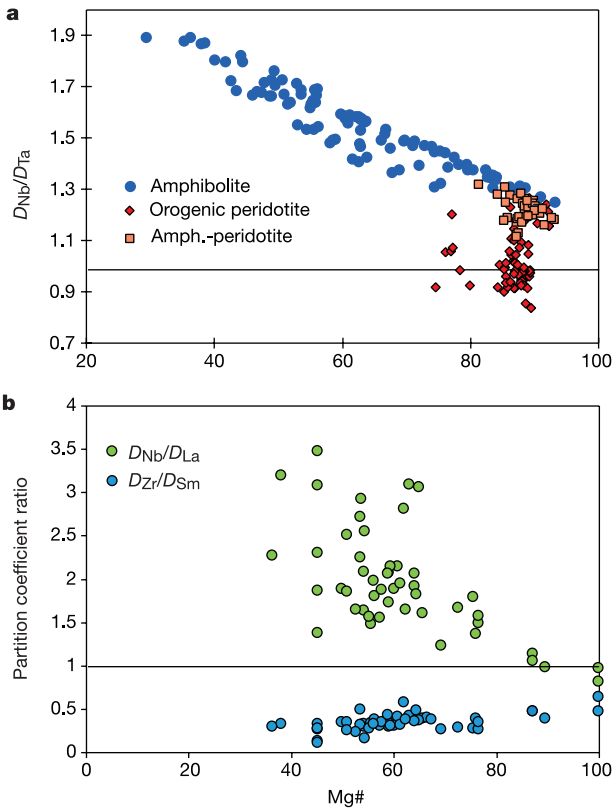

Figure 2 Trace-element ratios in amphiboles as a function of Mg# (= 100 Mg/(Mg + Fe)). **a**, D_{Nb}/D_{Ta} ratios are calculated using the equation given in the text together with the Mg# and Ti contents from microprobe analyses of natural and experimental amphiboles. Plotted as a function of Mg#, we can see that only amphiboles with Mg# below about 70 can fractionate Nb from Ta significantly, producing the required low Nb/Ta in coexisting melts. Amphiboles with Mg# 80–90, modelled here by amphiboles in peridotites (natural and experimental), cannot fractionate Nb from Ta. This would apply to high-Mg# amphibolites that may result from metamorphism of mafic to ultramafic cumulates in the lower oceanic crust. **b**, Partition coefficient ratios from our experiments[11–13] show that the lower-Mg# amphiboles also fractionate Nb from La (green circles) and Zr from Sm (blue circles), whereas amphiboles with Mg# > 80 cannot. Melts derived by melting of amphibolites with low Mg# will therefore have a more significant trough in the incompatible element pattern at Nb and Ta. The values plotted in **b** are from the same experiments used to calibrate the predictive expression for D_{Nb}/D_{Ta} applied in **a**.

not likely to reach deeper than the uppermost 3 or 4 km (ref. 10).

We now contrast the behaviour of trace elements during melting of amphibolite and eclogite on the basis of recent experimental trace-element partitioning studies. Current models for the genesis of TTG, the continental crust and adakites require garnet in the residue to explain low concentrations of heavy rare-earth elements (HREE), for which both garnet amphibolite and eclogite melting provide reasonable solutions[1,4]. The behaviour of the high-field-strength elements (HFSE) Nb, Ta, Zr and Hf are now sufficiently well known to assess critical ratios involving these elements. The amphibole partitioning data are taken from our detailed experimental studies at 1.4 GPa pressure, in which trace-element determinations in mineral-glass pairs in experimental run products by ion microprobe were combined with crystal structure refinements for all experimentally synthesized amphiboles, so that the site preferences and incorporation mechanisms of trace elements are well-defined[11–13]. This is particularly important for understanding the partitioning behaviour of the HFSE, as it can be shown that amphibole decouples Nb and Ta from Zr and Hf. Nb and Ta are located on the M1 site, charge-balancing dehydrogenation of the amphiboles (exchange of O^{2-} for OH^-), whereas Zr (and Hf) are not related to dehydrogenation and occur on the M2 site[12,13]. The partitioning behaviour for the eclogite minerals garnet, clinopyroxene and rutile is taken from experiments on tonalite[14,15], and those for the other amphibolite minerals plagioclase and orthopyroxene from previous studies[16–20]. Almost all partition coefficients (D) used are obtained using *in situ* analyses of minerals and glass by either ion microprobe or laser ablation inductively coupled plasma mass spectrometry (ICP-MS).

An important result of the amphibole study is that the ionic radii of Nb and Ta are not identical as almost universally assumed, but that Ta is about 0.015 Å smaller[12]. This means that in any mineral in which these two elements occupy a site smaller than Ta, low D_{Nb}/D_{Ta} (<1) will occur in that mineral: this is confirmed for rutile by experimental measurements where both partition coefficients have been determined[21,22]. In contrast, the effective size of the M1 site in amphibole straddles the ionic radii of Nb and Ta, with the result that D_{Nb}/D_{Ta} is higher than 1 for low-Mg# amphiboles[12]. Thus, where rutile dominates the Nb-Ta budget, as for rutile-bearing eclogites, high Nb/Ta is to be expected in melts.

In Fig. 1b, the Nb/Ta and Zr/Sm ratios of melts produced from amphibolites and eclogites are compared for the extreme cases of batch and pure fractional melting. Results are shown for eclogites with and without 0.5% rutile: the latter would be relevant only for exceptionally depleted basalt compositions, as recent experiments have shown that rutile saturation should be achieved during partial melting[23]. This is consistent with the almost ubiquitous occurrence of rutile in Archaean eclogite xenoliths[24,25]. For the amphibolites, measured modal mineralogies from suprasolidus experiments on melting of basalt at 0.8, 1.0 and 1.6 GPa were used (Fig. 1b)[4,5]. Amphibole is a residual mineral in all of these. The 0.8-GPa assemblage is garnet-free and orthopyroxene-bearing, whereas the higher-pressure assemblages contain garnet and clinopyroxene in addition to amphibole and plagioclase. The vertical array of symbols (Fig. 1b) shows that all model melts can explain high Zr/Sm relative to mantle values, but that only amphibolite models can explain low Nb/Ta. The ratios for melts of eclogite, especially with rutile, do not fit that of TTG, the bulk continental crust, adakites or most modern island-arc basalts. Whereas melting of rutile-bearing eclogite can explain low HREE concentrations and high Zr/Sm, it fails the critical Nb/Ta test. Batch melts (1–15%) of all three amphibolites lie in the lower right quadrant, as do pure fractional melts at degrees of melting below 10% (all melts to 15% in the case the 0.8-GPa amphibolite). Batch melting may be the more realistic model given the relatively high SiO_2 content of the melts.

During melting of amphibolites, Nb/Ta in the melt is controlled by the Mg# and titanium concentration of the amphiboles, and can be predicted from microprobe analyses using the following expression: $\ln({}^{Amph/L}D_{Nb/Ta}) = 2.45 - 1.26Mg - 0.84Ti$ ($r^2 = 0.84$; ${}^{Amph/L}D_{Nb/Ta}$ is the partition coefficient ratio for Nb and Ta between amphibole and melt; average difference between calculated and observed ratios was 7%, maximum 20%; ref. 12). Application of this equation to a compilation of amphibole compositions from amphibolites and peridotites shows that only amphiboles with Mg# less than about 70 can cause low Nb/Ta in coexisting melts (Fig. 2a), and that the fractionation increases with decreasing Mg# of the amphibole. These low-Mg# amphiboles are also able to cause the greatest fractionation between Nb/La and Zr/Sm (Fig. 2b). In contrast, amphiboles with Mg# > 80 cannot impart low Nb/Ta to coexisting melts, nor can they cause low Nb/La. We conclude that the trace-

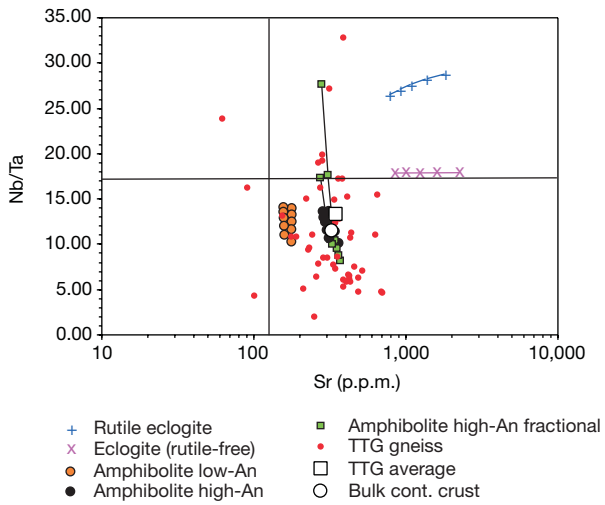

Figure 3 Modelling of Sr concentrations in melts of amphibolite and eclogite. The high calculated Sr concentrations in melts of eclogite, with (blue plus signs) or without rutile (pink crosses), further supports the conclusion that TTG (shown as an average and as individual rocks) cannot have originated by melting of eclogite. Melts from amphibolite fit better, whereby the Sr concentration depends on D_{Sr}, which itself is inversely proportional to the anorthite content of plagioclase[19]. The 'high-An' amphibolites which produce the best fit may result from high water contents during melting[27]. The starting composition used for modelling was the same average Archaean basalt as in Fig. 1b with 157 p.p.m. Sr (ref. 30). Use of a lower Sr concentration such as in modern MORB (113 p.p.m.) would not change the conclusions appreciably; the bulk partition coefficient for Sr is the controlling factor. The intersection of the black lines indicates primitive mantle values for reference.

element characteristics of TTG, including low Nb/Ta and Nb/La and high Zr/Sm, can be explained by melting of amphibolite in the subducting slab where amphiboles have relatively low Mg#, but not by melting of Mg-rich amphibolites or eclogites in the lower parts of thick oceanic crust. The decoupling of Nb and Ta from Zr and the fractionation of Nb from Ta in low-Mg# amphiboles is the best explanation for the production of melts in the lower right quadrant of Fig. 1; no other mantle phase with this capability has been reported.

Melting of rutile eclogite cannot be (or have been) volumetrically important in the production of igneous rocks at convergent margins, apart, perhaps, from the production of relatively rare alkaline volcanics with high Nb/Ta[26]. Many eclogite xenoliths are thought to represent former oceanic crust that melted during subduction[24,25], and many have high Nb/Ta rutiles[25]. Our results show that those with high Nb/Ta cannot have formed with rutile coexisting with melt, but must have melted as rutile-free amphibolites, followed by solid-state transformation of amphibolite to rutile eclogite on further subduction. This must also apply to the supposed lost eclogite reservoir with high Nb/Ta that may be located deep in the mantle[25].

Although melting of garnet amphibolite with amphibole Mg# of 40–50 and plagioclase with 40–50% anorthite end member (An_{40-50}) can explain the low HREE, high Zr/Sm and low Nb/Ta of the early continental crust, minor refinements to the model may be necessary for some trace elements, notably Sr, U and Th. The predicted melts from all amphibolite melting models shown in Fig. 1b have U and Th contents that are higher than TTG and the bulk continental crust, indicating that D_U and D_{Th} are too low in the models by a factor of about 3. This may be due to underestimation of the modal proportion of amphibole and/or plagioclase (see Fig. 1b), or to incorrect estimation of D_U and D_{Th} for plagioclase[20]. The problem for the more abundant trace element strontium is more acute (Fig. 3). D_{Sr} is inversely proportional to the anorthite content of plagioclase, as parameterized by Blundy and Wood[19]. The 'low-An' circles in Fig. 3 are for the 1.0- and 1.6-GPa amphibolites from Fig. 1b with $D_{Sr} = 5.25$, corresponding to plagioclase with An_{45}. Using a lower D_{Sr} of 2, corresponding to a more Ca-rich plagioclase, excellent agreement results for Sr concentrations in average TTG and bulk continental crust in a model otherwise identical to the low-An model. This correction is not arbitrary, as it is notoriously difficult to attain equilibrium in experiments on plagioclase, and it has been shown that the presence of water results in a considerable increase in the anorthite content of plagioclase[27]. The partitioning data used for plagioclase[18,19] are based on experiments without water. The calculations for melting of eclogite in Fig. 3 confirm that the early continental crust is not related to melting of eclogite.

These results also eliminate the melting of amphibole peridotite[28] as a possible cause of the low Nb/Ta in modern island-arc volcanics (Fig. 1a), because the high Mg# of amphiboles from mantle wedge assemblages above the subducting slab prevents fractionation of Nb from Ta (Fig. 2a). A recent study of fluids released by antigorite breakdown in deeply subducted mantle shows that they do not display relative enrichment in large ion lithophile elements compared to HFSE, thus strongly supporting the hypothesis that HFSE are soluble in natural subduction fluids[29]. Amphibole may nevertheless cause the low Nb/La and low Nb/Ta signatures of arc magmas: low-Mg#, low-Ti amphiboles may crystallize from slab-derived, silica-rich aqueous fluids at high fluid/rock ratios, causing Nb depletion relative to La and Ta in residual fluids. These move further and progressively equilibrate with peridotite mantle at lower fluid/rock ratios, while migrating to the regions where large-scale melting of the wedge occurs. During melting of amphibole peridotite, amphibole is no longer able to fractionate Nb from Ta or La to an appreciable extent. □

Received 4 October 2001; accepted 16 May 2002; doi:10.1038/nature00799.

1. Drummond, M. S. & Defant, M. J. A model for trondhjemite-tonalite-dacite genesis and crustal growth via slab melting: Archean to modern comparisons. *J. Geophys. Res.* **95,** 21503–21521 (1990).
2. Kröner, A. Evolution of the Archean continental crust. *Annu. Rev. Earth Planet. Sci.* **13,** 49–74 (1985).
3. Martin, H. in *Archean Crustal Evolution* (ed. Condie, K. C.) 205–259 (Elsevier, Amsterdam, 1994).
4. Rapp, R. P., Watson, E. B. & Miller, C. F. Partial melting of amphibolite/eclogite and the origin of Archean trondhjemites and tonalites. *Precambr. Res.* **51,** 1–25 (1991).
5. Wolf, M. B. & Wyllie, P. J. Dehydration-melting of amphibolite at 10 kbar: the effects of temperature and time. *Contrib. Mineral. Petrol.* **115,** 369–383 (1994).
6. Martin, H. Adakitic magmas: modern analogues of Archean granitoids. *Lithos* **46,** 411–429 (1998).
7. Karsten, J. L., Klein, E. M. & Sherman, S. B. Subduction zone geochemical characteristics in ocean ridge basalts from the southern Chile ridge: implications of modern ridge subduction systems for the Archean. *Lithos* **37,** 143–161 (1996).
8. Saunders, A. D., Tarney, J., Kerr, A. C. & Kent, R. W. The formation and fate of large oceanic igneous provinces. *Lithos* **37,** 81–95 (1996).
9. Arndt, N. T. *et al.* Were komatiites wet? *Geology* **26,** 739–742 (1998).
10. Bickle, M. J., Nisbet, E. G. & Martin, A. Archean greenstone belts are not oceanic crust. *J. Geol.* **102,** 121–138 (1994).
11. Bottazzi, P. *et al.* Distinct site preferences for heavy and light rare-earth elements and the prediction of $^{Amph/L}D_{REE}$. *Contrib. Mineral. Petrol.* **137,** 36–45 (1999).
12. Tiepolo, M. *et al.* Nb and Ta incorporation and fractionation in titanian pargasite and kaersutite: crystal-chemical constraints and implications for natural systems. *Earth Planet. Sci. Lett.* **176,** 185–201 (2000).
13. Tiepolo, M., Bottazzi, P., Foley, S. F., Oberti, R. & Zanetti, A. Fractionation of Nb and Ta from Zr and Hf at mantle depths: the role of titanian-pargasite and kaersutite. *J. Petrol.* **42,** 221–232 (2001).
14. Barth, M. G., Foley, S. F. & Horn, I. Partial melting in Archean subduction zones: constraints from experimentally determined trace-element partition coefficients between eclogitic minerals and tonalitic melts under upper mantle conditions. *Precambr. Res.* **113,** 323–340 (2002).
15. Foley, S. F., Barth, M. G. & Jenner, G. A. Rutile/melt partition coefficients for trace elements and an assessment of the influence of rutile on the trace element characteristics of subduction zone magmas. *Geochim. Cosmochim. Acta* **64,** 933–938 (2000).
16. Kennedy, A. K., Lofgren, G. E. & Wasserburg, G. J. An experimental study of trace element partitioning between olivine, orthopyroxene and melt in chondrules: equilibrium values and kinetic effects. *Earth Planet. Sci. Lett.* **115,** 177–195 (1993).
17. Eggins, S. M., Rudnick, R. L. & McDonough, W. F. The composition of peridotites and their minerals: a laser-ablation ICP-MS study. *Earth Planet. Sci. Lett.* **154,** 53–71 (1998).
18. Bindemann, I. N., Davis, A. M. & Drake, M. J. Ion microprobe study of plagioclase-basalt partition experiments at natural concentration levels of trace elements. *Geochim. Cosmochim. Acta* **62,** 1175–1193 (1998).
19. Blundy, J. D. & Wood, B. J. Crystal-chemical controls on the partitioning of Sr and Ba between plagioclase feldspar, silicate melts, and hydrothermal solutions. *Geochim. Cosmochim. Acta* **55,** 193–209 (1991).
20. Dunn, T. & Sen, C. Mineral/matrix partition coefficients for orthopyroxene, plagioclase, and olivine in basaltic to andesitic systems: a combined analytical and experimental study. *Geochim. Cosmochim. Acta* **58,** 717–733 (1994).
21. Green, T. H. & Pearson, N. J. An experimental study of Nb and Ta partitioning between Ti-rich minerals and silicate liquids at high pressure and temperature. *Geochim. Cosmochim. Acta* **51,** 55–62 (1987).
22. Jenner, G. A. *et al.* Determination of partition coefficients for trace elements in high-pressure-temperature experimental run products by laser ablation microprobe - inductively coupled mass spectrometry (LAM-ICP-MS). *Geochim. Cosmochim. Acta* **57,** 5099–5103 (1993).
23. Klemme, S., Blundy, J. D. & Wood, B. J. Experimental constraints on major and trace element partitioning during partial melting of eclogite. *Geochim. Cosmochim. Acta* (in the press).
24. Jacob, D. E. & Foley, S. F. Evidence for Archean oceanic crust with low high field strength element signature from diamondiferous eclogite xenoliths. *Lithos* **48,** 317–336 (1999).
25. Rudnick, R. L., Barth, M., Horn, I. & McDonough, W. F. Rutile-bearing refractory eclogites: Missing link between continents and depleted mantle. *Science* **287,** 278–281 (2000).
26. Stolz, A. J., Jochum, K. P., Spettel, B. & Hofmann, A. W. Fluid- and melt-related enrichment in the subarc mantle: evidence from Nb/Ta variations in island arc basalts. *Geology* **24,** 587–590 (1996).
27. Panjasawatwong, Y., Danyushevsky, L. V., Crawford, A. J. & Harris, K. L. An experimental study of the effects of melt composition on plagioclase-melt equilibria at 5 and 10 kbar: implications for the origin of magmatic high-An plagioclase. *Contrib. Mineral. Petrol.* **118,** 420–432 (1995).
28. Ionov, D. A. & Hofmann, A. W. Nb-Ta-rich mantle amphiboles and micas: implications for subduction-related metasomatic trace element fractionations. *Earth Planet. Sci. Lett.* **131,** 341–356 (1995).
29. Scambelluri, M. *et al.* Incompatible element-rich fluids released by antigorite breakdown in deeply subducted mantle. *Earth Planet. Sci. Lett.* **192,** 457–470 (2001).
30. Rollinson, H. R. Petrology and geochemistry of metamorphosed komatiites and basalts from the Sula Mountains greenstone belt Sierra Leone. *Contrib. Mineral. Petrol.* **134,** 86–101 (1999).

Acknowledgements

Discussions with R. Oberti, M.G. Barth and D.E. Jacob helped to shape the findings reported here.

Competing interests statement

The authors declare that they have no competing financial interests.

Correspondence and requests for materials should be addressed to S.F. (e-mail: sfoley@uni-greifswald.de).